

# Toward Task Generalization via Memory Augmentation in Meta-Reinforcement Learning

Kaixi Bao<sup>1</sup>, Chenhao Li<sup>2</sup>, Yarden As<sup>2</sup>, Andreas Krause<sup>3</sup>, Marco Hutter<sup>1</sup>

**Abstract**—In reinforcement learning (RL), agents often struggle to perform well on tasks that differ from those encountered during training. This limitation presents a challenge to the broader deployment of RL in diverse and dynamic task settings. In this work, we introduce memory augmentation, a memory-based RL approach to improve task generalization. Our approach leverages task-structured augmentations to simulate plausible out-of-distribution scenarios and incorporates memory mechanisms to enable context-aware policy adaptation. Trained on a predefined set of tasks, our policy demonstrates the ability to generalize to unseen tasks through memory augmentation without requiring additional interactions with the environment. Through extensive simulation experiments and real-world hardware evaluations on legged locomotion tasks, we demonstrate that our approach achieves zero-shot generalization to unseen tasks while maintaining robust in-distribution performance and high sample efficiency.

## I. INTRODUCTION

Reinforcement learning (RL) has made significant strides in training agents to perform complex tasks [1, 2, 3, 4, 5], achieving high performance in controlled settings. However, RL agents often struggle when faced with tasks outside their training distribution—a limitation known as the out-of-distribution (OOD) generalization challenge. This limitation restricts the applicability of RL policies to a broader range of tasks beyond those explicitly encountered during training [6, 7].

A common way to address this challenge is to increase training diversity to better encompass potential testing conditions. Domain randomization [8, 9, 10], for instance, achieves this by varying environment parameters, thereby exposing agents to a wide range of scenarios during training. However, as the extent of randomization increases, this method often suffers from reduced sample efficiency [11]. Additionally, increased variations during training can result in over-conservative strategies, especially in environments where these variations are not fully observable. In such settings, the agent may struggle to discern the current task parameterizations and only executes conservative moves, thereby sacrificing optimality. This raises a crucial question: how can an RL agent achieve robust performance across diverse environment variations, or tasks, without being explicitly exposed to them during training?

A promising method to improve the generalization of the policy is through experience augmentation [12], where training experiences are augmented to simulate a broader range of potential test-time conditions. However, pure augmentation,

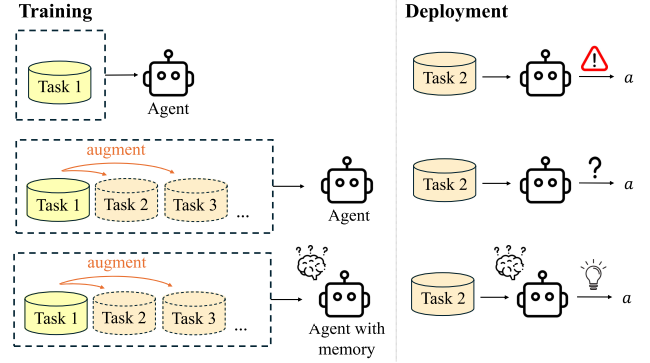


Fig. 1: Improving task generalization through memory augmentation. Top row: RL agents often struggle with tasks not encountered during training, leading to poor performance. Middle row: Experience augmentation expands the range of training scenarios to include potential test-time tasks; however, in partially observable settings, agents may fail to identify the current task parameterizations, resulting in over-conservative behavior. Bottom row: Incorporating memory mechanisms enables agents to infer task context, facilitating context-aware decision-making and improved adaptability.

without properly accounting for task context, may similarly cause over-conservativeness resulting from exposing the policy to excessive unobservable variations. Building on the contextual modeling capability of Recurrent Neural Networks (RNNs), which have been shown to effectively address partial observability [13], we enhance experience augmentation in RL by incorporating memory mechanisms that respect the necessary task context, as shown in Fig. 1.

In this work, we introduce *memory augmentation*, a novel approach to improve task generalization by augmenting training experience to simulate plausible OOD tasks and incorporating memory mechanisms to facilitate zero-shot task adaptation. Our approach trains a single unified policy that can perform well across both in-distribution (ID) and unseen OOD tasks.

In summary, our contributions include:

- We propose *memory augmentation*, a novel approach to improve task generalization without additional interactions with the environment.
- We validate our approach across a variety of legged locomotion experiments. Results demonstrate that our memory-augmented policies generalize effectively to unseen OOD tasks while maintaining robust ID performance.

<sup>1</sup>Department of Mechanical and Process Engineering, ETH Zurich, Switzerland.

<sup>2</sup>ETH AI Center, ETH Zurich, Switzerland.

<sup>3</sup>Department of Computer Science, ETH Zurich, Switzerland.  
{kaibao, chenhli, yardas, krausea, mahutter}@ethz.ch

Additionally, while maintaining comparable performance, they achieve superior sample efficiency compared to randomization-based policies, where the agent is explicitly trained across all conditions.

- We demonstrate the sim-to-real transfer of the learned memory-augmented policy on a quadrupedal robot for position tracking under joint failure. The robot successfully tracks the goals while effectively adapting to both ID and OOD joint failures.

## II. RELATED WORK

### A. Task generalization in RL

In RL, task generalization arises as a challenge when the agent is required to perform well on tasks that differ from those encountered during training. These differences may stem from variations in scenes, states, or reward structures [14]. Domain randomization, originally introduced for sim-to-real transfer in robotics [8, 9, 10], addresses this issue by randomizing environment parameters during training to encompass a broader range of potential test-time conditions. In robotic control, this often involves dynamics randomization, where parameters like masses, friction coefficients, joint damping, and actuator gains are varied during training to enhance policy robustness [10, 1, 2, 3, 15]. While this effectively broadens the agent’s exposure to diverse conditions, increased randomization often leads to reduced sample efficiency [11].

Alternatively, many works incorporate known physics principles or state structures into task design to approach task generalization. Examples include foot-placement dynamics [16], object invariance [17], granular media interactions [18], frequency domain parameterization [7], rigid body dynamics [19], and semi-structured Lagrangian dynamics models [20].

### B. Experience augmentation

While many data augmentation techniques in RL have focused on augmenting image-based observations to improve generalization across visual changes [21, 22, 23, 24], fewer studies have investigated augmentation at the induced state-action trajectory level—referred to as *experience augmentation*—which is the focus of our work.

One example of experience augmentation is PlayVirtual [25], which augments cycle-consistent virtual trajectories by leveraging forward and backward dynamics models in a latent space to improve feature representation learning. Meanwhile, in HER [12], which aims to address the sparse reward problem in RL, failed trajectories are transformed into meaningful learning signals through goal relabeling. This relabeling mechanism, as implemented in HER and its extensions [26, 27, 28, 29], can also be viewed as a form of experience augmentation. However, these approaches primarily focus on improving learning efficiency with limited training data rather than explicitly addressing task generalization.

In legged locomotion control, symmetry-based augmentation has been applied to state-action trajectories to encourage symmetry-invariant behavior [30, 31]. Inspired by these works, our approach leverages the inherent task structure to augment

state-action trajectories, generating synthetic experience of novel scenarios to enhance task generalization.

### C. Meta-RL

Meta-RL enables agents to quickly adapt to new tasks by leveraging experience gained during meta-training. Through exposure to multiple related tasks, the agent learns a context-aware policy [32, 33, 34, 35] or a good initialization [36, 37, 38], which allows it to adapt to novel, unseen tasks with minimal additional training [39]. In the field of memory-based meta-RL, RNNs have been widely employed for their ability to capture task context from past interactions, enabling zero-shot adaptation [32, 33]. Building on this framework, Nagabandi et al. [40] developed a dynamics model prior to enable rapid online adaptation in dynamic environments, while Zargarbashi et al. [41] trained a morphology-agnostic locomotion policy for legged robots.

## III. PRELIMINARIES

### A. Partially observable Markov Decision Process and Meta-RL

We model the problem as a Partially Observable Markov Decision Process (POMDP). We define a POMDP as the tuple  $\mathcal{M} = (\mathcal{S}, \mathcal{O}, \mathcal{A}, p, r, \gamma, \rho_0)$ , where  $\mathcal{S}$  is the set of states,  $\mathcal{O}$  is the set of observations,  $\mathcal{A}$  is the set of actions,  $p : \mathcal{S} \times \mathcal{A} \times \mathcal{S} \rightarrow [0, 1]$  is the state transition function,  $r : \mathcal{S} \times \mathcal{A} \rightarrow \mathbb{R}$  is the reward function,  $\gamma$  is the discount factor, and  $\rho_0 : \mathcal{S} \rightarrow [0, 1]$  is the initial state distribution.

In POMDPs, observations provide only partial information about the true underlying state, requiring the agent to reason about the task context. In conventional RL, the agent aims to learn a policy  $\pi$  that maximizes the expected cumulative reward:

$$J(\pi) = \mathbb{E}_{\tau \sim p_{\pi}(\tau)} \left[ \sum_{t=0}^{\infty} \gamma^t r(s_t, a_t) \right],$$

where  $\tau = (s_0, a_0, s_1, \dots)$  represents a trajectory sampled from the POMDP  $\mathcal{M}$  under the policy  $\pi$ .

In this work, we frame the problem of learning across multiple tasks as a meta-RL problem, with the objective of optimizing over a distribution of tasks  $p(\mathcal{T})$ . In our setting, this corresponds to a distribution of POMDPs  $\mathcal{M}(\mathcal{T})$ . We focus on the scenario where each task  $T \in \mathcal{T}$  exhibits unique dynamics while sharing a common reward function. The goal is to learn a policy  $\pi$  that maximizes the expected cumulative reward across tasks:

$$J(\pi) = \mathbb{E}_{T \sim p(\mathcal{T}), \tau \sim p_{\pi}(\tau|T)} \left[ \sum_{t=0}^{\infty} \gamma^t r(s_t, a_t) \right].$$

### B. Proximal Policy Optimization

In this work, we apply Proximal Policy Optimization (PPO) [42] as the RL algorithm. At the  $k$ -th learning step, the agent collects trajectories by executing its policy, parameterized by  $\theta_k$ . To optimize the policy, PPO employs importance sampling to address the discrepancy between the current policy  $\pi_{\theta}(a_t | s_t)$  and the policy from the previous update  $\pi_{\theta_k}(a_t | s_t)$  used to collect the data. The policy gradient is expressed as:

$$\nabla_{\theta} J(\pi_{\theta}) = \mathbb{E}_{\tau \sim p_{\pi_{\theta_k}}} \left[ \sum_{t=0}^{\infty} \eta_t(\theta) A^{\pi_{\theta_k}} \nabla_{\theta} \log \pi_{\theta}(a_t | s_t) \right], \quad (1)$$

where  $\eta_t(\theta) = \frac{p_{\pi_{\theta}}(s_t)}{p_{\pi_{\theta_k}}(s_t)} \frac{\pi_{\theta}(a_t | s_t)}{\pi_{\theta_k}(a_t | s_t)}$  is the importance sampling weight, and  $A^{\pi_{\theta_k}} = A^{\pi_{\theta_k}}(s_t, a_t)$  is the advantage function under the policy  $\pi_{\theta_k}$ . To stabilize training, PPO optimizes a clipped surrogate loss  $L_{\text{clip}}(\theta)$  [42], which constrains the magnitude of policy updates. Additionally, Generalized Advantage Estimation (GAE) [43] is commonly used to compute the advantage function, balancing bias and variance for efficient learning.

### C. Problem statement

We consider a set of tasks  $\mathcal{T}$ , where  $\mathcal{T}_{\text{ID}} \subset \mathcal{T}$  represents the subset of tasks accessible during training, referred to as ID tasks. The remaining tasks,  $\mathcal{T}_{\text{OOD}} = \mathcal{T} \setminus \mathcal{T}_{\text{ID}}$ , constitute the set of unseen tasks that differ from the training tasks. In this work, we focus on a subset of these unseen tasks,  $\mathcal{T}_{\text{OOD}}^{\text{aug}} \subset \mathcal{T}_{\text{OOD}}$ , which can be effectively simulated through task-structured augmentations without requiring additional interactions with the environment. These tasks exhibit different dynamics from  $\mathcal{T}_{\text{ID}}$  while maintaining the same reward structure. Our goal is to train a single policy that can adapt and perform well across both  $\mathcal{T}_{\text{ID}}$  and  $\mathcal{T}_{\text{OOD}}^{\text{aug}}$ . This is formalized by maximizing the expected cumulative reward:

$$J(\pi) = \mathbb{E}_{T \sim p(\mathcal{T}_{\text{ID}} \cup \mathcal{T}_{\text{OOD}}^{\text{aug}}), \tau \sim p_{\pi}(\tau | T)} \left[ \sum_{t=0}^{\infty} \gamma^t r_T(s_t, a_t) \right].$$

During training, only partial observations are available for  $\mathcal{T}_{\text{ID}}$ . In this setting, the agent must infer the task context implicitly based on past observations and actions.

## IV. APPROACH

### A. Task-structured augmentation

To augment the training experience, our approach leverages a set of transformation functions, denoted by  $\mathcal{G}$ , where each  $g \in \mathcal{G}$  represents a transformation that reflects the underlying structure that we assume to exist in the task space. These transformations are used to generate synthetic experience in  $\mathcal{T}_{\text{OOD}}^{\text{aug}}$  from the original data collected in  $\mathcal{T}_{\text{ID}}$ .

Formally, let  $\tau = \{(o_t, a_t, o_{t+1}, r_t)\}_{t=0}^T$  represent a trajectory collected by the current policy  $\pi_{\theta_k}$  within the training set  $\mathcal{T}_{\text{ID}}$ . Each transformation  $g = (g_o, g_a) \in \mathcal{G}$  consists of functions  $g_o : \mathcal{O} \rightarrow \mathcal{O}$  and  $g_a : \mathcal{A} \rightarrow \mathcal{A}$ , which map an original observation-action pair  $(o, a)$  to a new pair  $(o^g, a^g) = (g_o(o), g_a(a))$ . We denote  $s_t^g$  as the latent state corresponding to the transformed observation  $o_t^g$ . For all  $g \in \mathcal{G}, s \in \mathcal{S}, a \in \mathcal{A}$ , it is assumed that the following properties hold:

(a) **Transition probability invariance:** The probability of reaching the next state from a given state-action pair remains identical in their respective tasks. Formally, this is expressed as:

$$T(s_{t+1}^g | s_t^g, a_t^g) = T(s_{t+1} | s_t, a_t).$$

(b) **Initial state distribution invariance:** The initial state distribution remains invariant across original and transformed trajectories. Formally, this is expressed as:

$$p_0(s^g) = p_0(s).$$

(c) **Reward invariance:** Each original state-action pair  $(s_t, a_t)$  and its transformed counterpart  $(s_t^g, a_t^g)$  receive the same rewards in their respective tasks. Formally, this is expressed as:

$$r(s_t^g, a_t^g) = r(s_t, a_t).$$

These properties ensure alignment between the original and transformed tasks, maintaining the coherence of task dynamics. The resulting augmented trajectory  $\tau_g = \{(o_t^g, a_t^g, o_{t+1}^g, r_t)\}_{t=0}^T$  represents the agent's simulated experience within an augmented task  $T \in \mathcal{T}_{\text{OOD}}^{\text{aug}}$ , generated without real environment interactions. The training dataset is then constructed as the union of the original and augmented trajectories:

$$\mathcal{D}_{\text{train}} = \mathcal{D}_{\text{ID}} \cup \mathcal{D}_{\text{OOD}}^{\text{aug}} = \{\tau_i\}_{i=1}^N \cup \bigcup_{g \in \mathcal{G}} \{\tau_i^g\}_{i=1}^N.$$

An example of such transformations in  $\mathcal{G}$  includes symmetry transformations, which have been used in RL for manipulation tasks [27] and legged locomotion control [30, 31]. Specifically, for quadrupedal robots, symmetry transformations can simulate mirrored conditions (e.g., joint failures) across left-right and front-back body parts. Similarly, for humanoid robots, they can replicate mirrored conditions across left-right body parts. These transformations leverage the morphological symmetry inherent to legged robots and uphold the essential invariance properties (a)–(c) [44].

### B. Training with augmented data

Following the method of Mittal et al. [30], we approach data augmentation in PPO by constructing augmented policies  $\pi_{\theta_k}^g$  such that  $\pi_{\theta_k}^g(a^g | s^g) = \pi_{\theta_k}(a | s), \forall g \in \mathcal{G}, s \in \mathcal{S}, a \in \mathcal{A}$ . Based on properties (a)–(c), it can be shown that for a state-action pair  $(s, a)$  and its transformed counterpart  $(s^g, a^g)$ , the following invariances hold [30]:

$$A^{\pi_{\theta_k}^g}(s^g, a^g) = A^{\pi_{\theta_k}}(s, a), \text{ and } p_{\pi_{\theta_k}^g}(s^g) = p_{\pi_{\theta_k}}(s). \quad (2)$$

Using Eq. 2, the policy update rule in Eq. 1 becomes

$$\begin{aligned} \nabla_{\theta} J(\pi_{\theta}) = & \mathbb{E}_{\tau \sim p_{\pi_{\theta_k}}} \left[ \sum_{t=0}^{\infty} \eta_t(\theta) A^{\pi_{\theta_k}} \nabla_{\theta} \log \pi_{\theta}(a_t | s_t) \right] \\ & + \sum_{g \in \mathcal{G}} \mathbb{E}_{\tau \sim p_{\pi_{\theta_k}}} \left[ \sum_{t=0}^{\infty} \eta_t^g(\theta) A^{\pi_{\theta_k}} \nabla_{\theta} \log \pi_{\theta}(a_t^g | s_t^g) \right], \end{aligned} \quad (3)$$

with  $\eta_t^g(\theta) = \frac{p_{\pi_{\theta}}(s_t^g)}{p_{\pi_{\theta_k}}(s_t)} \frac{\pi_{\theta}(a_t^g | s_t^g)}{\pi_{\theta_k}(a_t | s_t)}$ , which retains the action probability of the original data. For further details, we refer readers to [30].

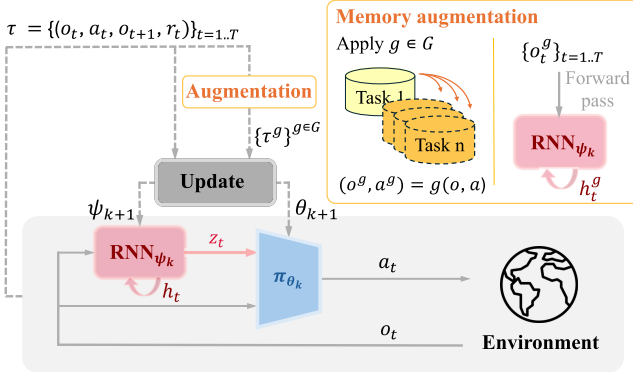


Fig. 2: Overview of our training framework.

For each gradient update, we sample a mini-batch of trajectories from the original rollouts along with their corresponding transformed trajectories:

$$\mathcal{D}_{\text{minibatch}} = \{\tau_i\}_{i=1}^{N_{\text{minibatch}}} \cup \bigcup_{g \in \mathcal{G}} \{\tau_i^g\}_{i=1}^{N_{\text{minibatch}}}.$$

This approach ensures balanced learning across both the original and augmented tasks, promoting equitable representation for each task during the policy update.

### C. Memory augmentation

While experience augmentation can enhance generalization by introducing greater training diversity, the resulting variations, combined with the partially observable nature of the environment, may cause the agent to adopt over-conservative strategies as it struggles to infer the latent task context. To address this limitation, we extend augmentation to the agent’s memory by incorporating an RNN into the training framework, as illustrated in Fig. 2. The RNN, leveraging its context modeling capability, acts as an implicit task encoder. At each time step, the RNN updates its hidden state  $h_t$  based on the observations, progressively capturing task-specific information accumulated so far. From this hidden state, the RNN generates a latent task embedding  $z_t$ , which conditions the policy, allowing it to adapt decisions based on the inferred context.

In addition to augmenting the trajectories, we extend the RNN’s hidden states to incorporate memory for the augmented tasks. As shown in Fig. 3, this is achieved by performing a forward pass with the transformed observation sequence  $(o_t^g)_{t=0}^T$  through the RNN. During this process, the RNN generates a sequence of hidden states  $(h_t^g)_{t=0}^T$  that progressively encode the evolving dynamics of the augmented observations. To ensure continuity in the context encoding, the initial hidden state  $h_0^{g,k}$  for the current update  $k$  is set to the final hidden state  $h_T^{g,k-1}$  from the previous update. The forward pass is performed continuously throughout the episode to ensure that the RNN’s hidden states capture the cumulative dynamics of the augmented observations at each step, providing an up-to-date context encoding for subsequent updates. The latent task embeddings  $(z_t^g)_{t=0}^T$ , generated from these hidden states,

provide the policy with the inferred context of the augmented tasks.

This memory augmentation allows the policy to infer unobservable context information for both ID and augmented scenarios. In contrast, a simple feedforward policy without memory relies solely on immediate partial observations and lacks the ability to infer latent task context, which may lead to degraded ID performance when augmented data is introduced.

Our training process incorporating memory augmentation is outlined in Algorithm 1.

---

### Algorithm 1 Recurrent PPO with Memory Augmentation

---

**Input:** Number of iterations  $N_{\text{iter}}$

**Output:** Optimal policy and RNN parameters  $\theta^*, \psi^*$

```

1: Initialize environment, policy  $\pi_\theta$  and RNN  $\psi$ ;
2: Initialize hyperparameters  $\epsilon, \gamma$ ;
3: Define transformation set  $\mathcal{G}$  for experience augmentation;
4: for  $k = 1, \dots, N_{\text{iter}}$  do
5:   Collect rollouts  $\mathcal{D}_{\text{ID}}$  using  $\pi_\theta$ ;
6:   Generate  $\mathcal{D}_{\text{aug}}^{\text{OOD}}$  by applying transformations  $g \in \mathcal{G}$ ;
7:   Update RNN hidden states via forward pass;
8:   Combine rollouts:  $\mathcal{D}_{\text{train}} \leftarrow \mathcal{D}_{\text{ID}} \cup \mathcal{D}_{\text{aug}}^{\text{OOD}}$ ;
9:   for  $\mathcal{D}_{\text{minibatch}}$  sampled from  $\mathcal{D}_{\text{train}}$  do
10:    Compute surrogate objective  $L_{\text{clip}}$ ;
11:    Update  $\theta$  and  $\psi$ ;
12:   end for
13: end for
14: return  $\theta^*, \psi^*$ 

```

---

## V. EXPERIMENTS

### A. Environment and task setup

We evaluate the performance of our approach across eight legged locomotion experiments with the ANYmal D quadruped and Unitree G1 humanoid robots in Issac Lab [45]. The experiments are designed around two core task settings: *position tracking* and *velocity tracking*, with variations introduced to simulate joint failures and payload distributions:

- **Joint failure:** A joint failure is simulated by disabling the motor torque.
- **Quadruped robot:** During training, a joint in the left front leg (LF HAA, LF HFE, or LF KFE) is randomly disabled, categorized as an ID joint failure. Joint failures in other legs are considered OOD failures.
- **Humanoid robot:** A joint in the left hip (pitch, roll, or yaw) is randomly disabled during training (ID). Joint failures in the right hip are considered as OOD.

For both robots, a joint failure occurs with an 80% probability during training.

- **Payload:** A payload is simulated by imposing a vertical external force.
- **Quadruped Robot:** During training, a payload with a mass uniformly sampled from [30 kg, 40 kg] is applied at a random position on the left front section of the robot’s base (ID). Payloads with the same mass range

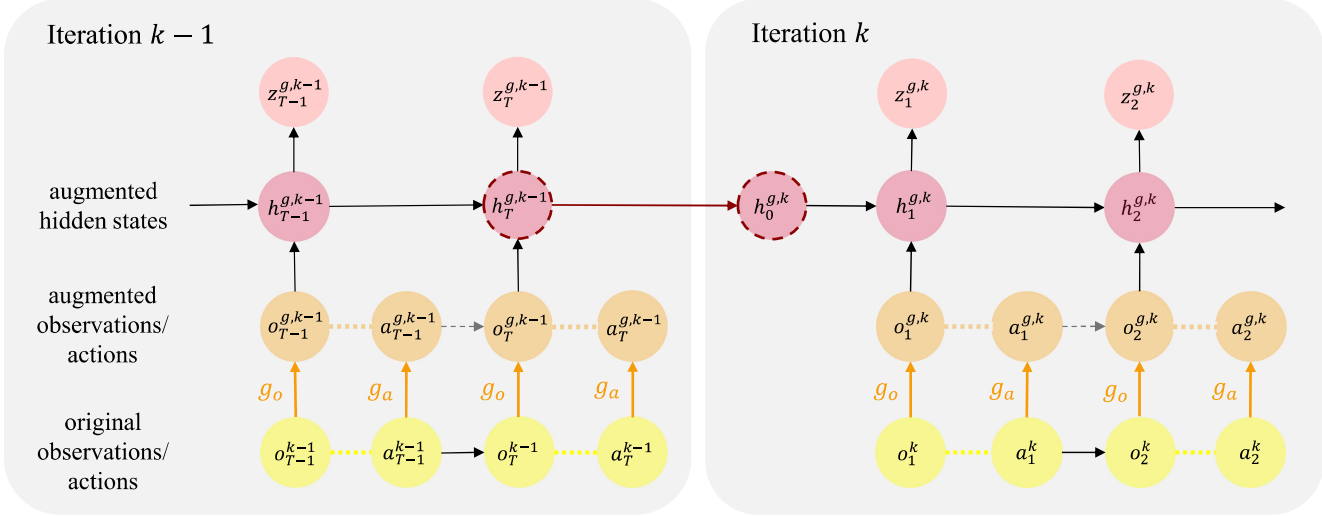


Fig. 3: Memory augmentation. Transformation  $g = (g_o, g_a) \in \mathcal{G}$  is applied to observations  $o_t$  and actions  $a_t^g$  to generate augmented observations  $o_t^g$  and actions  $a_t^g$ . The augmented observation sequence is forward passed through the RNN, producing hidden states  $h_t^g$ . During the  $k$ -th policy update, the initial augmented hidden state  $h_0^{g,k}$  is set to the last hidden state from the previous update  $h_T^{g,k-1}$ , ensuring continuity and context retention across updates.

applied to other sections of the base are considered OOD.

– **Humanoid Robot:** During training, a payload with a mass uniformly sampled from [40 kg, 50 kg] is applied at a random position on the left shoulder of the robot (ID). Payloads applied to the right shoulder are considered OOD.

We train a memory-based policy both with and without experience augmentation, referred to as **Memory-Aug** and **Memory-ID**, respectively. To assess the role of memory-based task inference, we also train a standard MLP policy with experience augmentation [30, 31], referred to as **Baseline-Aug**, and a standard MLP policy without augmentation, referred to as **Baseline-ID**.

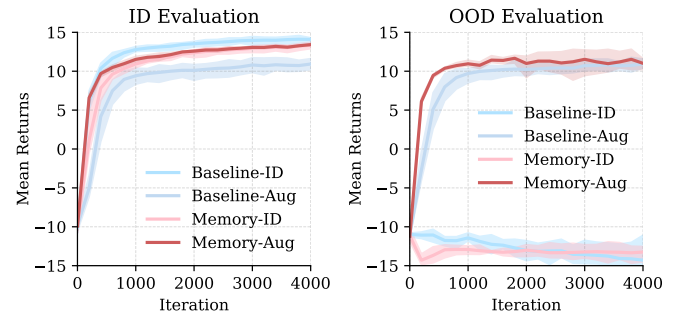
Additionally, we include randomization-based policies, where the agent is exposed to all variations mentioned above (ID + OOD) during training. These are referred to as **Baseline-Rand** for the MLP-only architecture and **Memory-Rand** for the memory-enabled architecture.

We include all implementation details in the Appendix, including observations, rewards, network architectures and hyperparameter values.

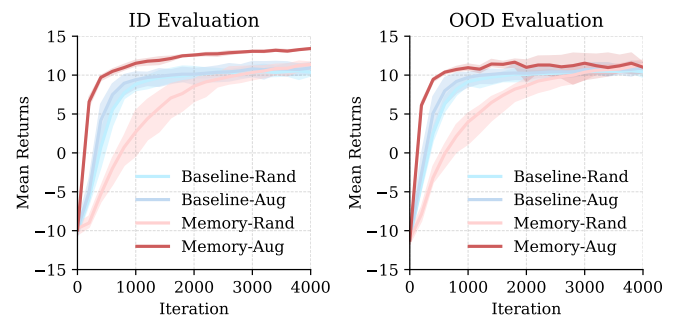
#### B. Task performance and data efficiency

We evaluate performance using the average episodic return, calculated as the mean of undiscounted cumulative rewards across 1000 episodes. Training for each policy was conducted using five different seeds. Figure 4 presents detailed evaluations of different policies in quadruped position tracking under both ID and OOD joint failure scenarios.

As shown in Fig. 4b, **Baseline-Aug** exhibits ID performance comparable to **Baseline-Rand**, but falls short of matching the



(a) Mean episodic returns with minimum and maximum values of policies trained **with and without augmentation**.



(b) Mean episodic returns with minimum and maximum values of **augmentation- and randomization-based policies**.

Fig. 4: Evaluation of quadruped position tracking under joint failure for different policies.

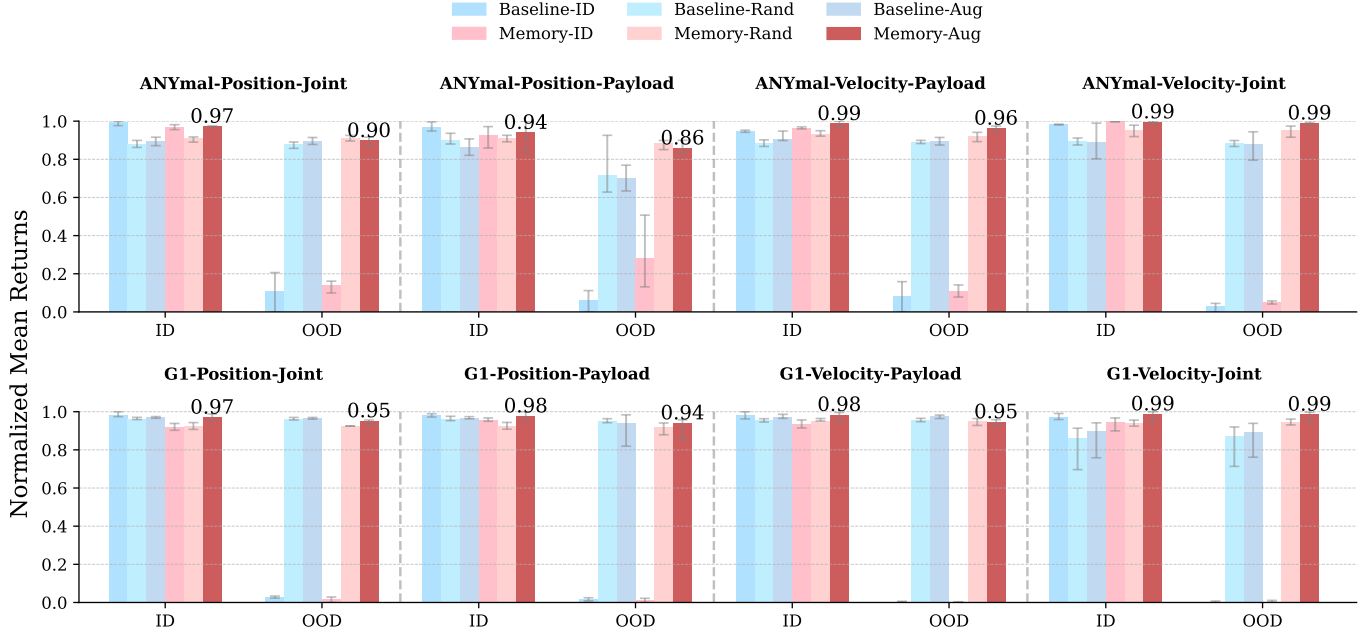


Fig. 5: Normalized mean episodic returns on ID and OOD tasks, with error bars indicating minimum and maximum values.

ID performance of **Baseline-ID** (see Fig. 4a). These findings underscore how variations introduced through randomization or augmentation can cause a simple MLP policy to adopt suboptimal behaviors in partially observable settings. Lacking the ability to infer latent task context from partial observations, such policies resort to over-conservative strategies, limiting their ability to optimize performance in specific tasks.

In contrast, **Memory-Aug** achieves performance comparable to **Memory-ID** on ID tasks, as shown in Fig. 4a. This result highlights how the memory module effectively captures task context from partial observations and utilizes this capability in experience augmentation, thereby preserving robust ID performance.

In Fig. 4b, **Memory-Aug** demonstrates performance on par with **Memory-Rand** in both ID and OOD tasks. Notably, **Memory-Aug** achieves this without requiring any additional environment interactions for these OOD tasks, demonstrating significantly higher sample efficiency than **Memory-Rand**.

To verify that these findings are not coincidental, we evaluate the approaches across all experiments. As shown in Fig. 5, the trend of ID performance degradation in **Baseline-Rand** and **Baseline-Aug** persists, particularly in experiments involving the quadruped robot, where task diversity is more pronounced. In contrast, **Memory-Rand** and **Memory-Aug** consistently achieve comparable ID performance to **Memory-ID**. This again highlights the importance of the memory mechanism in partially observable settings with substantial task diversity. By leveraging its context inference capability, this memory module allows the agent to maintain robust performance in ID tasks. Furthermore, **Memory-Aug** achieves performance comparable to **Memory-Rand** in both ID and OOD tasks. However, unlike **Memory-Rand**, **Memory-Aug** eliminates

the need for additional environment interactions, effectively improving sample efficiency.

### C. Behavior analysis with memory augmentation

We observe distinct strategies adopted by different policies for quadruped position tracking with impaired joint, particularly in response to HFE and KFE joint failures. Agents trained with **Baseline-Rand** and **Baseline-Aug** often attempt to walk directly toward the goal using very small steps, as shown in the left part of Fig. 6. This over-cautious behavior reflects a tendency to uniformly reduce reliance on all joints rather than identifying and compensating for the specific failed joint. Despite their careful movements, the joint impairment often leads to stumbling or passive change in body orientation during tracking.

In contrast, agents trained with **Baseline-ID** and **Memory-ID** demonstrate a more adaptive strategy under ID joint failure. They tend to first turn sideways toward the goal, then move laterally while dragging the impaired leg to minimize reliance on the failed joint (see upper row of Fig. 6). This intentional body orientation adjustment at the start enables them to maintain greater stability while effectively progressing toward the goal. Notably, agents trained with **Memory-Rand** and **Memory-Aug** exhibit similar adaptive behavior, as shown in the middle and bottom rows on the right side of Fig. 6.

To further support these findings, we conduct a quantitative analysis of feet air time, calculated as the total duration the feet remain off the ground, and feet contact frequency, measured as the total number of instances the feet make contact with the ground. These metrics provide insight into how effectively the agents adapted their motion to compensate for joint failures.

As illustrated in Fig. 7, in ID tasks, **Baseline-Rand** and

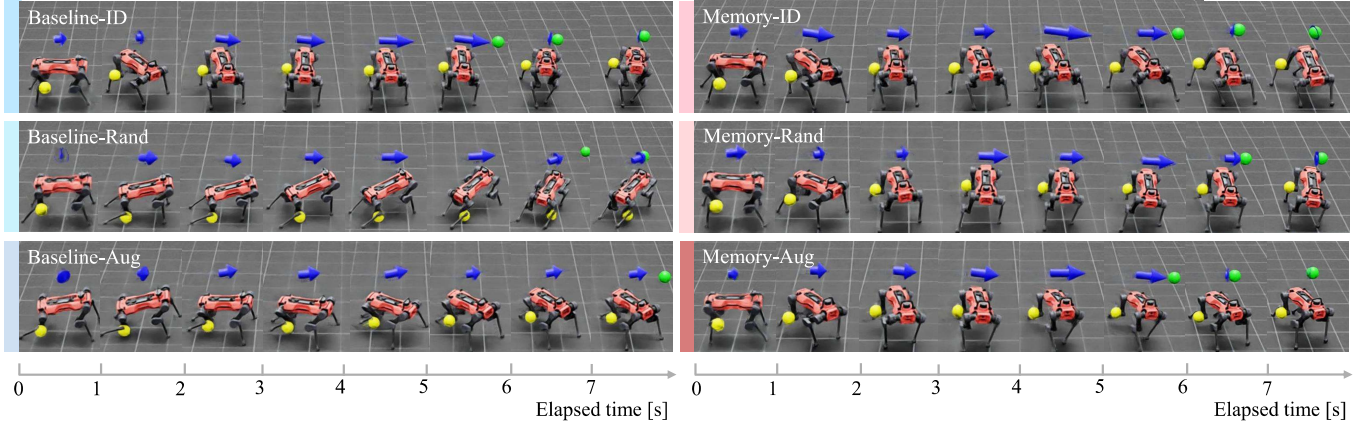


Fig. 6: Behavior analysis of different policies for quadruped position tracking under an ID KFE joint failure. The yellow marker denotes the impaired joint, the blue arrow represents the current base velocity, and the green marker indicates the goal position. Left: The **Baseline-ID**-trained agent actively turns sideways toward the goal within the first second, then moves laterally while dragging the impaired leg to minimize reliance on the failed joint. In contrast, agents trained with **Baseline-Rand** and **Baseline-Aug** attempt to walk directly toward the goal using very small steps. Failing to adapt to the joint failure, these agents often stumble and passively change their body orientation during tracking. Right: Agents trained with memory-enabled policies actively adjust their body orientation within the first second, effectively compensating for the impaired joint and maintaining stable locomotion.

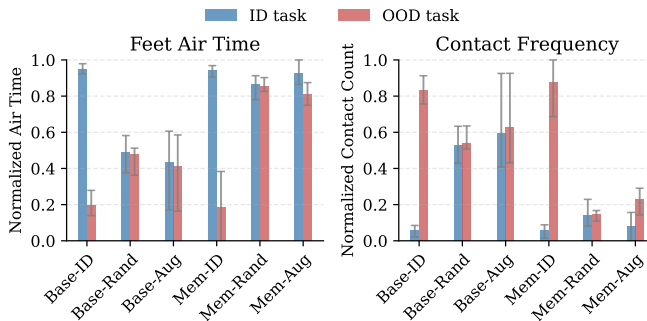


Fig. 7: Motion analysis. Normalized episodic feet air time and feet contact frequency for different policies in quadruped position tracking under ID and OOD joint failures, with error bars indicating minimum and maximum values.

**Baseline-Aug** demonstrate significantly shorter feet air time and more frequent ground contact compared to **Baseline-ID**. This aligns with our observation that agents employing these policies tend to take smaller, more cautious steps during goal tracking. This conservative behavior persists in OOD tasks, as evidenced by the low feet air time and high contact frequency of **Baseline-Rand** and **Baseline-Aug** under OOD joint failures. In contrast, **Memory-Rand** and **Memory-Aug** exhibit feet air time and contact frequency comparable to **Memory-ID** in ID tasks, while maintaining consistent levels in OOD tasks. This highlights the ability of **Memory-Rand** and **Memory-Aug** to effectively adapt their motion strategies in response to both ID and OOD joint failures.

We attribute this context-aware behavior to the memory-

based task inference capability provided by the RNN. By leveraging past experience, the RNN enables the agent to infer the underlying task context from partial observations, including the presence and nature of joint failures. This capability enables the agent to dynamically adapt its behavior across diverse scenarios, adopting strategies that compensate for impairments and optimize task performance.

## VI. HARDWARE EXPERIMENTS

We tested our **Memory-Aug** policy in position tracking under joint failure on the ANYmal D robot. To facilitate sim-to-real transfer, we introduced randomization in terrain profiles with a noise range of  $[0.0, 0.05]$  during training.

As shown in Figure 8 and the supplementary video, the robot successfully tracked multiple goals consecutively, while adapting effectively to both ID and OOD joint failures. These results demonstrate the ID robustness and OOD generalization of the memory-augmented policy on real robots.

Additionally, we also tested **Baseline-Aug** policy trained under the same terrain profiles. As shown in Figure 9, the robot exhibited limited adaptability under ID joint failure, frequently losing balance during goal tracking.

## VII. LIMITATIONS

The main limitation of our work lies in the reliance on prior knowledge of the task structure, which is essential for augmenting the training experience to simulate diverse task conditions. This dependency restricts the selection of transformations to those that satisfy the necessary invariance assumptions, potentially limiting generalization in cases where such assumptions are difficult to establish. That said, this

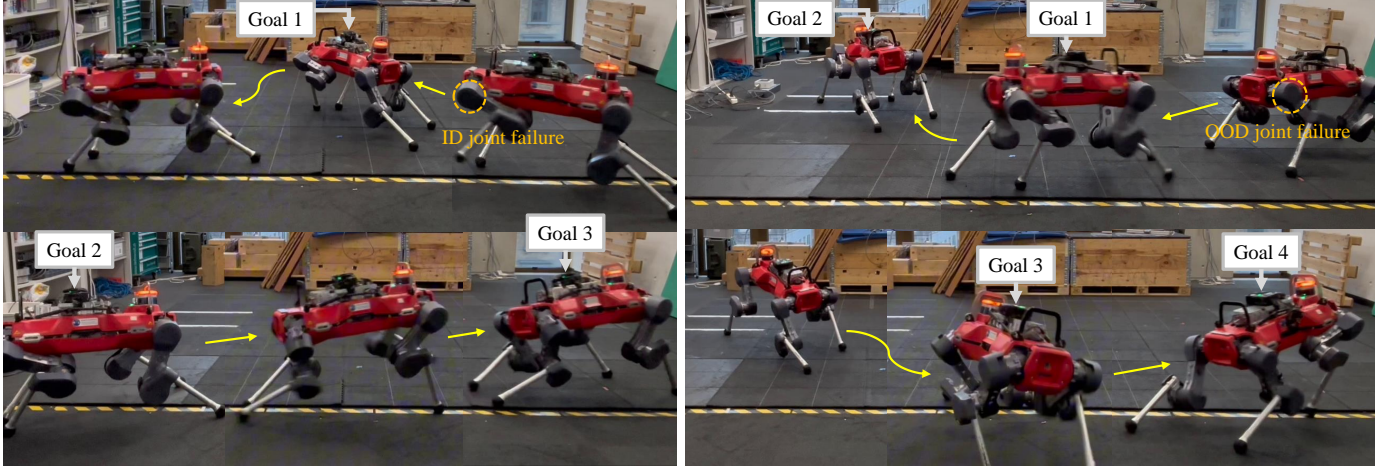


Fig. 8: Hardware experiment. Position tracking under ID (LF HAA) and OOD (RH HAA) joint failures with **Memory-Aug** policy.

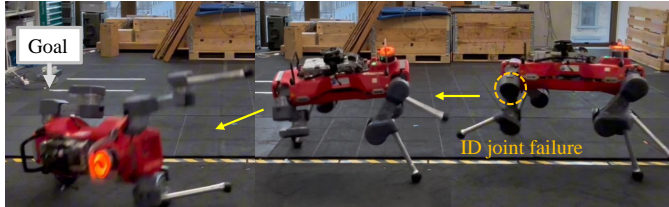


Fig. 9: Hardware experiment. Position tracking under ID (LF HAA) joint failure with **Baseline-Aug** policy.

reliance on prior knowledge also offers the advantage of systematically utilizing our understanding of the system’s dynamics. By incorporating domain-specific insights, we can design targeted transformations that align with the inherent properties of the task. In the future, we aim to broaden the applicability of our method by exploring more flexible augmentation techniques to simulate a wider range of OOD task conditions and enhance generalization across diverse and unstructured environments.

### VIII. CONCLUSION

In this work, we have presented an RL framework that integrates task-structured experience augmentation with memory mechanisms to enhance task generalization. By simulating varied task conditions through augmented training experiences and incorporating memory-based task inference, our approach trains a single unified policy capable of handling both ID and OOD tasks without additional environment interactions.

This framework effectively addresses the limitations of policies lacking context-awareness, which tend to adopt over-conservative strategies in highly randomized and partially observable environments. Through extensive simulation experiments, we demonstrate that our approach achieves zero-shot generalization to OOD tasks while maintaining robust ID performance.

Furthermore, our approach demonstrates performance comparable to domain randomization in both ID and OOD tasks, while the latter requiring explicit environment interactions for these tasks. Notably, our method achieves this without requiring additional environment interactions for the OOD tasks, thereby overcoming the sample inefficiency associated with domain randomization.

Crucially, the memory mechanism proves essential in partially observable settings with substantial task diversity, allowing the agent to infer task context from past interactions. This facilitates zero-shot task adaptation and ensures reliable performance across both ID and OOD tasks. Moreover, our hardware experiments on a quadruped robot validate the sim-to-real transfer, demonstrating that our policy performs well on both ID and OOD tasks in real-world scenarios.

We believe this work inspires further advancements in developing adaptive RL agents capable of handling the complexities and uncertainties of real-world environments.

## REFERENCES

[1] Joonho Lee, Jemin Hwangbo, Lorenz Wellhausen, Vladlen Koltun, and Marco Hutter. Learning quadrupedal locomotion over challenging terrain. *Science robotics*, 5(47):eabc5986, 2020. URL <https://www.science.org/doi/epdf/10.1126/scirobotics.abc5986>.

[2] Ashish Kumar, Zipeng Fu, Deepak Pathak, and Jitendra Malik. Rma: Rapid motor adaptation for legged robots. *arXiv preprint arXiv:2107.04034*, 2021. URL <https://arxiv.org/pdf/2107.04034.pdf>.

[3] Takahiro Miki, Joonho Lee, Jemin Hwangbo, Lorenz Wellhausen, Vladlen Koltun, and Marco Hutter. Learning robust perceptive locomotion for quadrupedal robots in the wild. *Science robotics*, 7(62):eabk2822, 2022. URL <https://www.science.org/doi/abs/10.1126/scirobotics.abk2822>.

[4] David Hoeller, Nikita Rudin, Dhionis Sako, and Marco Hutter. Anymal parkour: Learning agile navigation for quadrupedal robots. *Science Robotics*, 9(88):eadi7566, 2024. URL <https://www.science.org/doi/epdf/10.1126/scirobotics.adi7566>.

[5] Chenhao Li, Marin Vlastelica, Sebastian Blaes, Jonas Frey, Felix Grimminger, and Georg Martius. Learning agile skills via adversarial imitation of rough partial demonstrations. In *Conference on Robot Learning*, pages 342–352. PMLR, 2023. URL <https://proceedings.mlr.press/v205/li23b.html>.

[6] Chenhao Li, Sebastian Blaes, Pavel Kolev, Marin Vlastelica, Jonas Frey, and Georg Martius. Versatile skill control via self-supervised adversarial imitation of unlabeled mixed motions. In *2023 IEEE international conference on robotics and automation (ICRA)*, pages 2944–2950. IEEE, 2023. URL <https://ieeexplore.ieee.org/stamp/stamp.jsp?tp=&arnumber=10160421>.

[7] Chenhao Li, Elijah Stanger-Jones, Steve Heim, and Sangbae Kim. Fld: Fourier latent dynamics for structured motion representation and learning. *arXiv preprint arXiv:2402.13820*, 2024. URL <https://arxiv.org/pdf/2402.13820.pdf>.

[8] Josh Tobin, Rachel Fong, Alex Ray, Jonas Schneider, Wojciech Zaremba, and Pieter Abbeel. Domain randomization for transferring deep neural networks from simulation to the real world. In *2017 IEEE/RSJ international conference on intelligent robots and systems (IROS)*, pages 23–30. IEEE, 2017. URL <https://ieeexplore.ieee.org/stamp/stamp.jsp?tp=&arnumber=8202133>.

[9] Fereshteh Sadeghi and Sergey Levine. Cad2rl: Real single-image flight without a single real image. *arXiv preprint arXiv:1611.04201*, 2016. URL <https://arxiv.org/pdf/1611.04201.pdf>.

[10] Xue Bin Peng, Marcin Andrychowicz, Wojciech Zaremba, and Pieter Abbeel. Sim-to-real transfer of robotic control with dynamics randomization. In *2018 IEEE international conference on robotics and automation (ICRA)*, pages 3803–3810. IEEE, 2018. URL <https://ieeexplore.ieee.org/stamp/stamp.jsp?tp=&arnumber=8460528>.

[11] Robert Kirk, Amy Zhang, Edward Grefenstette, and Tim Rocktäschel. A survey of zero-shot generalisation in deep reinforcement learning. *Journal of Artificial Intelligence Research*, 76:201–264, 2023. URL <https://www.jair.org/index.php/jair/article/view/14174>.

[12] Marcin Andrychowicz, Filip Wolski, Alex Ray, Jonas Schneider, Rachel Fong, Peter Welinder, Bob McGrew, Josh Tobin, OpenAI Pieter Abbeel, and Wojciech Zaremba. Hindsight experience replay. *Advances in neural information processing systems*, 30, 2017. URL <https://proceedings.neurips.cc/paper/2017/hash/453fadbd8a1a3af50a9df4df899537b5-Abstract.html>.

[13] Nicolas Heess, Jonathan J Hunt, Timothy P Lillicrap, and David Silver. Memory-based control with recurrent neural networks. *arXiv preprint arXiv:1512.04455*, 2015. URL <https://arxiv.org/pdf/1512.04455.pdf>.

[14] Kaiyang Zhou, Ziwei Liu, Yu Qiao, Tao Xiang, and Chen Change Loy. Domain generalization: A survey. *IEEE Transactions on Pattern Analysis and Machine Intelligence*, 45(4):4396–4415, 2022. URL <https://ieeexplore.ieee.org/stamp/stamp.jsp?tp=&arnumber=9847099>.

[15] OpenAI: Marcin Andrychowicz, Bowen Baker, Maciek Chociej, Rafal Jozefowicz, Bob McGrew, Jakub Pachocki, Arthur Petron, Matthias Plappert, Glenn Powell, Alex Ray, et al. Learning dexterous in-hand manipulation. *The International Journal of Robotics Research*, 39(1):3–20, 2020. URL <https://journals.sagepub.com/doi/full/10.1177/0278364919887447>.

[16] Yuxiang Yang, Ken Caluwaerts, Atil Iscen, Tingnan Zhang, Jie Tan, and Vikas Sindhwani. Data efficient reinforcement learning for legged robots. In *Conference on Robot Learning*, pages 1–10. PMLR, 2020. URL <https://proceedings.mlr.press/v100/yang20a.html>.

[17] Cansu Sancaktar, Sebastian Blaes, and Georg Martius. Curious exploration via structured world models yields zero-shot object manipulation. *Advances in Neural Information Processing Systems*, 35:24170–24183, 2022. URL [https://proceedings.neurips.cc/paper\\_files/paper/2022/hash/98ecdc722006c2959babdbdeb22eb75-Abstract-Conference.html](https://proceedings.neurips.cc/paper_files/paper/2022/hash/98ecdc722006c2959babdbdeb22eb75-Abstract-Conference.html).

[18] Suyoung Choi, Gwanghyeon Ji, Jeongsoo Park, Hyeongjun Kim, Juhyeok Mun, Jeong Hyun Lee, and Jemin Hwangbo. Learning quadrupedal locomotion on deformable terrain. *Science Robotics*, 8(74):eade2256, 2023. URL <https://www.science.org/doi/epdf/10.1126/scirobotics.ade2256>.

[19] Yunlong Song, Sangbae Kim, and Davide Scaramuzza. Learning quadruped locomotion using differentiable simulation. *arXiv preprint arXiv:2403.14864*, 2024. URL <https://arxiv.org/pdf/2403.14864.pdf>.

[20] Jacob Levy, Tyler Westenbroek, and David Fridovich-Keil. Learning to walk from three minutes of real-world data with semi-structured dynamics models. *arXiv preprint arXiv:2410.09163*, 2024. URL <https://arxiv.org/pdf/2410.09163.pdf>.

[21] Misha Laskin, Kimin Lee, Adam Stooke, Lerrel Pinto, Pieter Abbeel, and Aravind Srinivas. Reinforcement learning with augmented data. *Advances in neural information processing systems*, 33:19884–19895, 2020. URL [https://proceedings.neurips.cc/paper\\_files/paper/2020/hash/e615c82aba461681ade82da2da38004a-Abstract.html](https://proceedings.neurips.cc/paper_files/paper/2020/hash/e615c82aba461681ade82da2da38004a-Abstract.html).

[22] Roberta Raileanu, Maxwell Goldstein, Denis Yarats, Ilya Kostrikov, and Rob Fergus. Automatic data augmentation for generalization in reinforcement learning. *Advances in Neural Information Processing Systems*, 34:5402–5415, 2021. URL <https://proceedings.neurips.cc/paper/2021/hash/2b38c2df6a49b97f706ec9148ce48d86-Abstract.html>.

[23] Nicklas Hansen and Xiaolong Wang. Generalization in reinforcement learning by soft data augmentation. In *2021 IEEE International Conference on Robotics and Automation (ICRA)*, pages 13611–13617. IEEE, 2021. URL <https://ieeexplore.ieee.org/document/9561103>.

[24] Kaixin Wang, Bingyi Kang, Jie Shao, and Jiashi Feng. Improving generalization in reinforcement learning with mixture regularization. *Advances in Neural Information Processing Systems*, 33:7968–7978, 2020. URL <https://proceedings.neurips.cc/paper/2020/hash/5a751d6a0b6eff05cfe51b86e5d1458e6-Abstract.html>.

[25] Tao Yu, Cuiling Lan, Wenjun Zeng, Mingxiao Feng, Zhizheng Zhang, and Zhibo Chen. Playvirtual: Augmenting cycle-consistent virtual trajectories for reinforcement learning. *Advances in Neural Information Processing Systems*, 34:5276–5289, 2021. URL <https://proceedings.neurips.cc/paper/2021/hash/2a38a4a9316c49e5a833517c45d31070-Abstract.html>.

[26] Meng Fang, Tianyi Zhou, Yali Du, Lei Han, and Zhengyou Zhang. Curriculum-guided hindsight experience replay. *Advances in neural information processing systems*, 32, 2019. URL <https://proceedings.neurips.cc/paper/2019/hash/83715fd4755b33f9c3958e1a9ee221e1-Abstract.html>.

[27] Yijong Lin, Jiancong Huang, Matthieu Zimmer, Yisheng Guan, Juan Rojas, and Paul Weng. Invariant transform experience replay: Data augmentation for deep reinforcement learning. *IEEE Robotics and Automation Letters*, 5(4):6615–6622, 2020. URL <https://ieeexplore.ieee.org/stamp/stamp.jsp?tp=&arnumber=9158366>.

[28] Rui Yang, Meng Fang, Lei Han, Yali Du, Feng Luo, and Xiu Li. Mher: Model-based hindsight experience replay. *arXiv preprint arXiv:2107.00306*, 2021. URL <https://arxiv.org/pdf/2107.00306>.

[29] Charles Packer, Pieter Abbeel, and Joseph E Gonzalez. Hindsight task relabelling: Experience replay for sparse reward meta-rl. *Advances in neural information processing systems*, 34:2466–2477, 2021. URL <https://proceedings.neurips.cc/paper/2021/hash/1454ca2270599546dfcd2a3700e4d2f1-Abstract.html>.

[30] Mayank Mittal, N. Rudin, Victor Klemm, Arthur Allshire, and Marco Hutter. Symmetry considerations for learning task symmetric robot policies. *2024 IEEE International Conference on Robotics and Automation (ICRA)*, pages 7433–7439, 2024. URL <https://arxiv.org/pdf/2403.04359>.

[31] Zhi Su, Xiaoyu Huang, Daniel Ordoñez-Apaza, Yunfei Li, Zhongyu Li, Qiayuan Liao, Giulio Turrisi, Massimiliano Pontil, Claudio Semini, Yi Wu, et al. Leveraging symmetry in rl-based legged locomotion control. *arXiv e-prints*, pages arXiv–2403, 2024. URL <https://arxiv.org/pdf/2403.17320>.

[32] Yan Duan, John Schulman, Xi Chen, Peter L Bartlett, Ilya Sutskever, and Pieter Abbeel. RL<sup>2</sup>: Fast reinforcement learning via slow reinforcement learning. *arXiv preprint arXiv:1611.02779*, 2016. URL <https://arxiv.org/pdf/1611.02779>.

[33] Jane X Wang, Zeb Kurth-Nelson, Dhruva Tirumala, Hubert Soyer, Joel Z Leibo, Remi Munos, Charles Blundell, Dharshan Kumaran, and Matt Botvinick. Learning to reinforcement learn. *arXiv preprint arXiv:1611.05763*, 2016. URL <https://arxiv.org/pdf/1611.05763>.

[34] Nikhil Mishra, Mostafa Rohaninejad, Xi Chen, and Pieter Abbeel. A simple neural attentive meta-learner. *arXiv preprint arXiv:1707.03141*, 2017. URL <https://arxiv.org/pdf/1707.03141>.

[35] Luckeciano C Melo. Transformers are meta-reinforcement learners. In *international conference on machine learning*, pages 15340–15359. PMLR, 2022. URL <https://proceedings.mlr.press/v162/melo22a.html>.

[36] Chelsea Finn, Pieter Abbeel, and Sergey Levine. Model-agnostic meta-learning for fast adaptation of deep networks. In *International conference on machine learning*, pages 1126–1135. PMLR, 2017. URL <https://proceedings.mlr.press/v70/finn17a.html>.

[37] Zhenguo Li, Fengwei Zhou, Fei Chen, and Hang Li. Meta-sgd: Learning to learn quickly for few-shot learning. *arXiv preprint arXiv:1707.09835*, 2017. URL <https://arxiv.org/pdf/1707.09835>.

[38] Luisa Zintgraf, Kyriacos Shiarli, Vitaly Kurin, Katja Hofmann, and Shimon Whiteson. Fast context adaptation via meta-learning. In *International Conference on Machine Learning*, pages 7693–7702. PMLR, 2019. URL <https://proceedings.mlr.press/v97/zintgraf19a.html>.

[39] Jacob Beck, Risto Vuorio, Evan Zheran Liu, Zheng Xiong, Luisa Zintgraf, Chelsea Finn, and Shimon Whiteson. A survey of meta-reinforcement learning. *arXiv preprint arXiv:2301.08028*, 2023. URL <https://arxiv.org/pdf/2301.08028>.

[40] Anusha Nagabandi, Ignasi Clavera, Simin Liu, Ronald S Fearing, Pieter Abbeel, Sergey Levine, and Chelsea Finn. Learning to adapt in dynamic, real-world environments through meta-reinforcement learning. *arXiv preprint arXiv:1803.11347*, 2018. URL <https://arxiv.org/pdf/1803.11347>.

[41] Fatemeh Zargarbashi, Fabrizio Di Giuro, Jin Cheng, Dongho Kang, Bhavya Sukhija, and Stelian Coros. Metalooco: Universal quadrupedal locomotion with meta-reinforcement learning and motion imitation. *arXiv*

*preprint arXiv:2407.17502*, 2024. URL <https://arxiv.org/pdf/2407.17502.pdf>.

- [42] John Schulman, Filip Wolski, Prafulla Dhariwal, Alec Radford, and Oleg Klimov. Proximal policy optimization algorithms. *arXiv preprint arXiv:1707.06347*, 2017. URL <https://arxiv.org/pdf/1707.06347.pdf>.
- [43] John Schulman, Philipp Moritz, Sergey Levine, Michael Jordan, and Pieter Abbeel. High-dimensional continuous control using generalized advantage estimation. *arXiv preprint arXiv:1506.02438*, 2015. URL <https://arxiv.org/pdf/1506.02438.pdf>.
- [44] Daniel Ordoñez-Apaez, Giulio Turrisi, Vladimir Kostic, Mario Martin, Antonio Agudo, Francesc Moreno-Noguer, Massimiliano Pontil, Claudio Semini, and Carlos Mastalli. Morphological symmetries in robotics. *arXiv preprint arXiv:2402.15552*, 2024. URL <https://arxiv.org/pdf/2402.15552.pdf>.
- [45] Mayank Mittal, Calvin Yu, Qinxi Yu, Jingzhou Liu, Nikita Rudin, David Hoeller, Jia Lin Yuan, Ritvik Singh, Yunrong Guo, Hammad Mazhar, et al. Orbit: A unified simulation framework for interactive robot learning environments. *IEEE Robotics and Automation Letters*, 8(6):3740–3747, 2023. URL <https://ieeexplore.ieee.org/stamp/stamp.jsp?tp=&arnumber=10107764>.
- [46] Nikita Rudin, David Hoeller, Marko Bjelonic, and Marco Hutter. Advanced skills by learning locomotion and local navigation end-to-end. In *2022 IEEE/RSJ International Conference on Intelligent Robots and Systems (IROS)*, pages 2497–2503. IEEE, 2022. URL <https://ieeexplore.ieee.org/stamp/stamp.jsp?tp=&arnumber=9981198>.

## APPENDIX

### A. Implementation details

Our experiments focus on two primary task settings:

- **Position tracking:** The robot’s objective is to track a target position, sampled uniformly in polar coordinates with a radius between 1 m and 5 m around its initial position (i.e.,  $r \sim U([1.0, 5.0])$ ,  $\theta \sim U([-\pi, \pi])$ ). The target position is dynamically converted to Cartesian coordinates  $\mathbf{x}_b^{\text{cmd}} = [x_{b,x}^{\text{cmd}}, x_{b,y}^{\text{cmd}}] \in \mathbb{R}^2$ , relative to the robot’s base frame based on its current position. This relative target position is provided as input to the policy, which outputs the target joint position  $\mathbf{q}^*$ . The episode length is set to 8 s.
- **Velocity tracking:** The robot’s objective is to track a velocity command,  $\mathbf{v}^{\text{cmd}} = [v_x^{\text{cmd}}, v_y^{\text{cmd}}, \omega_z^{\text{cmd}}] \in \mathbb{R}^3$ , where  $v_x^{\text{cmd}}$  and  $v_y^{\text{cmd}}$  represent the target forward and lateral linear velocities, and  $\omega_z^{\text{cmd}}$  denotes the target yaw angular velocity. At the start of each episode, the velocity commands are sampled as follows:
  - **ANYmal quadruped robot:** The forward and lateral linear velocities are sampled uniformly between  $-1.0$  and  $1.0$  m/s:

$$v_x^{\text{cmd}} \sim U([-1.0, 1.0]), \quad v_y^{\text{cmd}} \sim U([-1.0, 1.0]).$$

- **G1 humanoid robot:** The forward linear velocity is sampled uniformly between  $0.0$  and  $1.0$  m/s:

$$v_x^{\text{cmd}} \sim U([0.0, 1.0]),$$

while the lateral velocity is fixed at zero:

$$v_y^{\text{cmd}} = 0.0.$$

A target heading direction is sampled uniformly from  $[-\pi, \pi]$ . The yaw command,  $\omega_z^{\text{cmd}}$ , is dynamically computed based on the target and current heading. The policy is trained to output the target joint position  $\mathbf{q}^*$ .

Tables S1–S6 summarize the observations, reward terms and training details for the two task settings.

TABLE S1: Position tracking observations

Term	Notation	Dimension	Units	Noise
<b>Observations</b>				
Base linear velocity	$\mathbf{v}_t$	3	m/s	[-0.10, 0.10]
Base angular velocity	$\boldsymbol{\omega}_t$	3	rad/s	[-0.20, 0.20]
Projected gravity	$\mathbf{g}_t^{\text{proj}}$	3	-	[-0.05, 0.05]
Joint position	$\mathbf{q}_t$	12   37	rad	[-0.01, 0.01]
Joint velocity	$\dot{\mathbf{q}}_t$	12   37	rad/s	[-1.50, 1.50]
Previous action	$\mathbf{a}_{t-1}$	12   37	rad	-
Remaining time	$t_{\text{left}}$	1	-	-
<b>Commands</b>				
Target xy position	$\mathbf{x}_{b,xy}^{\text{cmd}}$	2	m	-

TABLE S2: Velocity tracking observations

Term	Notation	Dimension	Units	Noise
<b>Observations</b>				
Base linear velocity	$\mathbf{v}_t$	3	m/s	[-0.10, 0.10]
Base angular velocity	$\boldsymbol{\omega}_t$	3	rad/s	[-0.20, 0.20]
Projected gravity	$\mathbf{g}_t^{\text{proj}}$	3	-	[-0.05, 0.05]
Joint position	$\mathbf{q}_t$	12   37	rad	[-0.01, 0.01]
Joint velocity	$\dot{\mathbf{q}}_t$	12   37	rad/s	[-1.50, 1.50]
Previous action	$\mathbf{a}_{t-1}$	12   37	rad	-
<b>Commands</b>				
Linear x velocity	$v_x^{\text{cmd}}$	1	m/s	-
Linear y velocity	$v_y^{\text{cmd}}$	1	m/s	-
Angular yaw velocity	$\omega_z^{\text{cmd}}$	1	rad/s	-

### B. Evaluation details

The feet air time metric, shown in Fig. 6, is calculated as the total duration the feet remain off the ground, expressed as:

$$\sum_{j=1}^{n_{\text{feet}}} (t_{\text{air},j} - 0.5) \cdot \mathbf{1}_{\text{new-contact},j}$$

The contact frequency measures the total number of times the feet make contact with the ground and is given by:

$$\sum_{j=1}^{n_{\text{feet}}} \mathbf{1}_{\text{new-contact},j}$$

TABLE S4: Velocity tracking reward terms

TABLE S3: Position tracking reward terms (adapted from Rudin et al. [46])

Term	Equation	Weight ANYmal	Weight G1
<b>Task</b>			
Target position tracking	$(1 - 0.5 \cdot \ \mathbf{x}_{b,xy}^{\text{cmd}}\ ^2) \cdot \mathbf{1}_{\{t > T-3\}}$	10.0	10.0
<b>Stability</b>			
Linear z velocity	$v_z^2$	-2.0	-0.2
Angular roll-pitch velocity	$\ \boldsymbol{\omega}_{xy}\ ^2$	None	-0.005
Flat orientation	$\ \mathbf{g}_{xy}^{\text{proj}}\ ^2$	-1.0	-1.0
Joint limits	$\ \mathbf{q} - \text{clip}(\mathbf{q}, \mathbf{q}_{\min}, \mathbf{q}_{\max})\ _1$	None	-1.0
Joint deviation (hip)	$\ \mathbf{q}_{\text{hip}} - \mathbf{q}_{\text{default,hip}}\ _1$	None	-0.1
Joint deviation (arms)	$\ \mathbf{q}_{\text{arms}} - \mathbf{q}_{\text{default,arms}}\ _1$	None	-0.1
Joint deviation (fingers)	$\ \mathbf{q}_{\text{fingers}} - \mathbf{q}_{\text{default,fingers}}\ _1$	None	-0.05
Joint deviation (torso)	$\ \mathbf{q}_{\text{torso}} - \mathbf{q}_{\text{default,torso}}\ _1$	None	-0.1
Applied torque limits	$\ \boldsymbol{\tau} - \boldsymbol{\tau}_{\text{computed}}\ _1$	-0.2	-0.2
Joint velocity	$\ \dot{\mathbf{q}}\ ^2$	-0.001	-0.001
Joint velocity limits	$\ \dot{\mathbf{q}} - \text{clip}( \dot{\mathbf{q}} , 0.9 \cdot \dot{\mathbf{q}}_{\max})\ _1$	-1.0	-1.0
Contact forces	$\ \max(\ \mathbf{f}_{\text{contact}}\  - 700, 0)\ _1$	-1.0e-5	-1.0e-5
Collision	$\ \max\left(\frac{\ \mathbf{f}_{\text{contact}}\ }{200}, 1\right)\ _1$	-0.5	None
Feet slide	$\sum_{j=1}^{n_{\text{feet}}} \ \mathbf{v}_{\text{foot},j}\  \cdot \mathbf{1}_{\text{contact},j}$	None	-0.1
<b>Smoothness</b>			
Joint torques	$\ \boldsymbol{\tau}\ ^2$	-1.0e-5	-2.0e-6
Joint accelerations	$\ \ddot{\mathbf{q}}\ ^2$	None	-1.0e-7
Action rate	$\ \mathbf{a}_t - \mathbf{a}_{t-1}\ ^2$	-0.01	-0.005
Feet air time	$\sum_{j=1}^{n_{\text{feet}}} (t_{\text{air},j} - t_{\text{thres}}) \cdot \mathbf{1}_{\text{new-contact},j}$	0.125	0.75
Base acceleration	$\ \dot{\mathbf{v}}_{\text{base}}\ ^2 + 0.02 \cdot \ \boldsymbol{\omega}_{\text{base}}\ ^2$	-0.001	None
Feet acceleration	$\sum_{j=1}^{n_{\text{feet}}} \ \dot{\mathbf{v}}_{\text{foot},j}\ $	-0.002	None
<b>Auxiliary</b>			
Termination penalty	$\mathbf{1}_{\text{terminated}}$	None	-200.0

Note:  $t_{\text{thres}} = 0.5$  for ANYmal and  $t_{\text{thres}} = 0.4$  for G1.

Term	Equation	Weight ANYmal	Weight G1
<b>Task</b>			
Linear xy velocity	$\exp(-\ \mathbf{v}_{xy} - \mathbf{v}_{xy}^{\text{cmd}}\ ^2/0.25)$	1.0	1.0
Angular yaw velocity	$\exp(-(\omega_z - \omega_z^{\text{cmd}})^2/0.25)$	0.5	1.0
<b>Stability</b>			
Linear z velocity	$v_z^2$	-2.0	-0.2
Angular roll-pitch velocity	$\ \boldsymbol{\omega}_{xy}\ ^2$	-0.05	-0.05
Flat orientation	$\ \mathbf{g}_{xy}^{\text{proj}}\ ^2$	-5.0	-1.0
Undesired contacts	$\mathbf{1}_{\text{self-collision}}$	-1.0	None
Joint limits	$\ \mathbf{q} - \text{clip}(\mathbf{q}, \mathbf{q}_{\min}, \mathbf{q}_{\max})\ _1$	None	-1.0
Joint deviation (hip)	$\ \mathbf{q}_{\text{hip}} - \mathbf{q}_{\text{default,hip}}\ _1$	None	-0.1
Joint deviation (arms)	$\ \mathbf{q}_{\text{arms}} - \mathbf{q}_{\text{default,arms}}\ _1$	None	-0.1
Joint deviation (fingers)	$\ \mathbf{q}_{\text{fingers}} - \mathbf{q}_{\text{default,fingers}}\ _1$	None	-0.05
Joint deviation (torso)	$\ \mathbf{q}_{\text{torso}} - \mathbf{q}_{\text{default,torso}}\ _1$	None	-0.1
Feet slide	$\sum_{j=1}^{n_{\text{feet}}} \ \mathbf{v}_{\text{foot},j}\  \cdot \mathbf{1}_{\text{contact},j}$	None	-0.1
<b>Smoothness</b>			
Joint torques	$\ \boldsymbol{\tau}\ ^2$	-2.5e-5	-2.0e-6
Joint accelerations	$\ \ddot{\mathbf{q}}\ ^2$	-2.5e-7	-1.0e-7
Action rate	$\ \mathbf{a}_t - \mathbf{a}_{t-1}\ ^2$	-0.01	-0.005
Feet air time	$\sum_{j=1}^{n_{\text{feet}}} (t_{\text{air},j} - t_{\text{thres}}) \cdot \mathbf{1}_{\text{new-contact},j}$	0.5	0.75
<b>Auxiliary</b>			
Termination penalty	$\mathbf{1}_{\text{terminated}}$	None	-200.0

Note:  $t_{\text{thres}} = 0.5$  for ANYmal and  $t_{\text{thres}} = 0.4$  for G1.

TABLE S5: Position tracking training details

Hyperparameter	ANYmal	G1
<b>PPO hyperparameters</b>		
Parallel environments	4,096	4,096
Steps per environment	48	48
Epochs per update	5	5
Minibatches per epoch	4	4
Discount rate ( $\gamma$ )	0.99	0.99
GAE parameter	0.95	0.95
Value loss coefficient	1.0	1.0
Clipping parameter	0.20	0.20
Entropy coefficient	0.005	0.003
Maximum gradient norm	1.00	1.00
Initial learning rate	0.001	0.001
Target KL	0.01	0.01
Optimizer	Adam	Adam
<b>Policy Network architectures</b>		
Policy ( $\pi$ ) MLP hidden layers	128, 128, 128	256, 128, 128
Critic ( $V^\pi$ ) MLP hidden layers	128, 128, 128	256, 128, 128
MLP activations	ELU	ELU
<b>Memory Module</b>		
RNN type	LSTM	LSTM
RNN hidden size	256	256
RNN hidden layer	1	1

TABLE S6: Velocity tracking training details

Hyperparameter	ANYmal	G1
<b>PPO hyperparameters</b>		
Parallel environments	4,096	4,096
Steps per environment	24	24
Epochs per update	5	5
Minibatches per epoch	4	4
Discount rate ( $\gamma$ )	0.99	0.99
GAE parameter	0.95	0.95
Value loss coefficient	1.0	1.0
Clipping parameter	0.20	0.20
Entropy coefficient	0.005	0.008
Maximum gradient norm	1.00	1.00
Initial learning rate	0.001	0.001
Target KL	0.01	0.01
Optimizer	Adam	Adam
<b>Policy Network architectures</b>		
Policy ( $\pi$ ) MLP hidden layers	128, 128, 128	256, 128, 128
Critic ( $V^\pi$ ) MLP hidden layers	128, 128, 128	256, 128, 128
MLP activations	ELU	ELU
<b>Memory Module</b>		
RNN type	LSTM	LSTM
RNN hidden size	256	512
RNN hidden layer	1	1